A Revisit of Orbital Angular Momentum Multiplexing in Multipath Environment

Wei Xue, Xiaoming Chen, Xiaobo Liu, Xiangshuai Meng, Anxue Zhang, Wei E. I. Sha

***Abstract*—It is commonly believed that orbital angular momentum (OAM) multiplexing is only suitable for short-range communications in line-of-sight (LoS) scenario and multipath propagation would be detrimental for OAM communications. It has been demonstrated very recently that OAM multiplexing could work in rich isotropic multipath environment when the conventional spatial equalization is used for data detection. Moreover, the resulting channel capacity is comparable to that of a conventional multiple-input multiple-output system. Nevertheless, the rich isotropic multipath environment is an ideal multipath scenario. In this paper, we investigate the performance of OAM multiplexing in arbitrary multipath environment. Contrary to the common belief, it is shown that multipath can be beneficial for OAM multiplexing in terms of channel capacity. Particularly, the OAM capacity increases with enlarged angular spread of the channel and reaches its maximum when the angular spread is comparable to the divergence angle of the OAM beam. Based on the study, the OAM multiplexing is further investigated for base station (BS) applications. It is shown that OAM based BS antennas are comparable to (or even outperform) the conventional BS antennas in terms of channel capacity.**

***Keywords*—multiplexing, multipath environment, orbital angular momentum (OAM)**

Manuscript received Aug. 11, 2020; revised Oct. 15, 2020; accepted Oct. 22, 2020. This work was supported in part by National Natural Science Foundation of China (No. 61801366), Natural Science Foundation of Shaanxi Province (No. 2020JM-078), and the Innovation Team Research Fund of Shaanxi Province (No. 2019TD-013). The associate editor coordinating the review of this paper and approving it for publication was W. C. Cheng.

W. Xue, X. M. Chen, X. B. Liu, X. S. Meng, A. X. Zhang. School of Information and Communications Engineering, Xi'an Jiaotong University, Xi'an 710049, China (e-mail: xuewei@stu.xjtu.edu.cn; xiaoming.chen@mail.xjtu.edu.cn; liu10052118@163.com; xsmeng@xjtu.edu.cn; anxuezhang@mail.xjtu.edu.cn).

W. E. I. Sha. College of Information Science and Electronic Engineering, Zhejiang University, Hangzhou 310027, China (e-mail: weisha@zju.edu.cn).

I. Introduction

Thanks to the orthogonality between different orbital angular momentum (OAM) modes[1-5], it has been found applications in wireless communications[6,7], radar imaging[8], source stirring[9], etc. Among these applications, there has been some debates over the conventional OAM communications[10]. The main concerns for the conventional OAM communications are the amplitude null in the beam center and the crosstalk due to misalignment or multipath. The former confines OAM to short-range communications, and the latter prevents OAM communications in multipath environments (this is the realistic scenarios for wireless communication). Due to these limitations, most investigations on OAM communications presume a pure line-of-sight (LoS) scenario[10-16]. Only few works explore the multipath effect on OAM communications[17,18]. It is concluded that the multipath has a detrimental effect on OAM multiplexing due to the induced crosstalk between OAM modes. While the statement is correct for the conventional OAM communication[2,5], it is worthy of pointing out that the crosstalk incurred by multipath can be significantly mitigated by the spatial equalizations (e.g., zero-forcing equalization)[19,20] of multiple-input multiple-output (MIMO) systems[21].

A hybrid orthogonal division multiplexing (HODM) scheme by combining OAM multiplexing and orthogonal frequency division multiplexing (OFDM) is proposed in Ref. [22]. By using the HODM scheme, the capacity of wireless communications can be drastically increased in sparse multipath environments. The plane spiral OAM-based MIMO (PSOAM-MIMO) systems are investigated in non-LOS (NLOS) scenarios[23], it is found that the PSOAM-MIMO system performs better than the LOS scenario, and outperforms the conventional MIMO system slightly. Very recently, it has been experimentally demonstrated that OAM communications perform well in multipath environments by combining OAM multiplexing with a conventional MIMO equalizer[21]. Nevertheless, the corresponding experimental verification in Ref. [21] was conducted in a reverberation chamber. It is well known that the reverberation chamber emulates a rich isotropic multipath environment[24], where the

propagation waves are isotopically distributed over the whole sphere from the view of statistical ray physics. Yet, the angular distribution of the propagation channel in real-life multipath environments is seldom isotropic. In fact, the propagation waves in real-life multipath environments are usually limited within a certain angular range (spread). This motivates us to investigate the performance of OAM communication (with the spatial equalization) in more realistic non-isotropic multipath environments.

In this work, we focus on the angular-spread effect on OAM multiplexing and conduct an in-depth investigation. Contrary to the common belief, it is shown that multipath can actually be beneficial for OAM multiplexing in terms of channel capacity. Specifically, the OAM capacity increases as the angular spread of the channel increases and reaches the maximum when the angular spread is comparable to the divergence angle of the OAM beam. Based on the study, the OAM communication is further investigated for base station (BS) applications. It is shown that OAM based BS antennas outperform the conventional BS antennas in terms of channel capacity in certain circumstances.

II. OAM Waves

As demonstrated by massive literatures, the electromagnetic (EM) wave carries not only the linear momentum but also the angular momentum. The angular momentum can be divided into the spin angular momentum (SAM) and the OAM. The SAM determines the polarization states of the EM wave, and OAM suggests a twist wavefront of the EM wave. Specifically, an OAM wave has a helical phase distribution $e^{-jl\varphi}$ (in which $l \in Z$ is the OAM mode number and φ is the transverse azimuthal angle) and a ring-shaped intensity with a null area in the center (when $l \neq 0$). SAM has only two orthogonal states. However, OAM has theoretically unlimited orthogonal modes, which allow for achieving higher spectral efficiency and channel capacity[25].

Various OAM generation techniques have been proposed and verified in the past decades, including Q-plate[26], uniform circular array (UCA)[11,12], spiral phase plate (SPP)[13,14], metasurface[15,16], etc. To facilitate simulation and analysis, exact expressions of the electric field of the generated OAM waves are required. Thus the circular traveling-wave antenna method[27] is adopted in this work.

Suppose a ring circuit with a radius of a is located in the horizontal plane. It is fed with a constant electric current amplitude I_0, but a consecutive phase along the circle of $l\varphi$ (where l is the mode number of the OAM wave to be generated, and φ is the azimuth angle). Obviously, the phase of the electric current varies $2l\pi$ over the complete ring circuit. The components of the electric field $\boldsymbol{E}(r,\theta,\varphi)$ (i.e., E_r, E_θ and E_φ) for an arbitrary observation point $P(r,\theta,\phi)$ in a spherical coordinate system can be calculated as[27]

$$\begin{cases} E_r = -\dfrac{C}{2\omega\varepsilon} e^{-jkr} e^{-jl\varphi} \dfrac{k\sin\theta}{r^2}[(J_{l-1}+J_{l+1}) + l(J_{l-1}-J_{l+1})], \\ E_\theta = \dfrac{C}{2\omega\varepsilon} e^{-jkr} e^{-jl\varphi} \cos\theta \left[\dfrac{jk^2}{r}(J_{l-1}+J_{l+1}) + \dfrac{kl}{r^2}(J_{l-1}-J_{l+1})\right], \\ E_\varphi = \dfrac{C}{2\omega\varepsilon} e^{-jkr} e^{-jl\varphi} \left[\dfrac{k^2}{r}(J_{l-1}-J_{l+1}) - \dfrac{jkl}{r^2}(J_{l-1}+J_{l+1})\right], \end{cases} \tag{1}$$

where $C = -j^l a I_0/2$, ε is the permittivity, k is the wavenumber, ω is the angular frequency. J_l is the lth order Bessel function of first kind, and the variable for Bessel functions is $ka\sin\theta$, θ is the elevation angle. Obviously, there exist only E_θ and E_φ in the far field situation.

Once we obtained the electric field in the far field, the radiation pattern can be further investigated using the radiation intensity[28]

$$U(\theta,\varphi) = U_\theta^2 + U_\varphi^2 = U_0[\cos^2\theta (J_{l-1}+J_{l+1})^2 + (J_{l-1}-J_{l+1})^2], \tag{2}$$

where U_θ and U_φ are two components of the radiation intensity in the far field, U_0 is a constant for a specific configuration of the circular traveling-wave antenna. Actually, for specific a and l, the angle of the main lobe can be calculated based on (2)

$$\theta_M = \arg\max_\theta \{U(\theta,\varphi)\}. \tag{3}$$

In order to have an intuitive understanding of the characteristics of OAM waves and the circular traveling-wave antenna method, some representative cases are simulated. Corresponding simulation results are very helpful for the analysis in the subsequent sections.

Fig. 1(a) shows the simulated radiation patterns of different OAM modes (i.e., $l \in [2,7]$) when $a = \lambda$. Obviously, the divergence angle grows larger when the OAM mode increases. The intensity of the main lobe decreases as the OAM mode increases. These can be easily explained by the characteristics of the Bessel functions[29]. In addition, the power of the side lobes against that of the main lobe varies much for different OAM modes. For example, the power of the side lobe is nearly comparable to that of the main lobe when $l = 3$. Fig. 1(b) shows the simulated radiation patterns of different radii of the ring circuits (i.e., $a = p\lambda$, $p \in [1,6]$) when $l = 3$. It can be seen that the divergence angle reduces with the radius of the ring circuit increased. Moreover, as the radius becomes larger, the power of the main lobe increases and that of the side lobes decreases.

To explore the relationship between the OAM modes, the radii of the ring circuits and the divergence angles, the simulated divergence angles as functions of OAM modes and radii

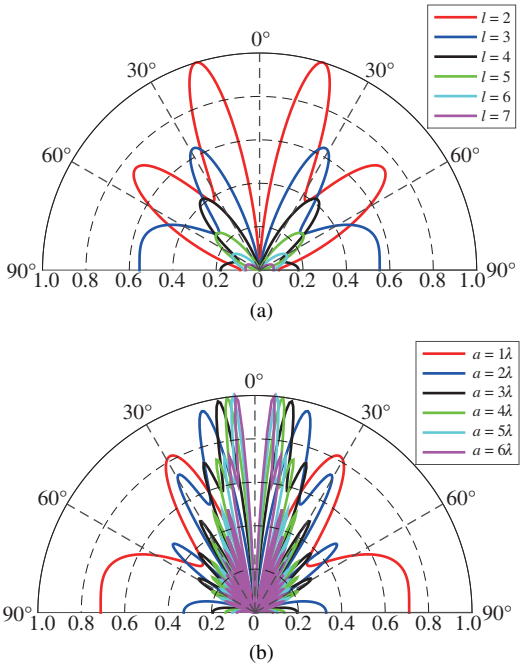

Figure 1 The simulated radiation patterns of (a) different OAM modes (i.e., $l \in [2,7]$) when $a = \lambda$; (b) different radii of the ring circuits (i.e., $a = p\lambda$, $p \in [1,6]$) when $l = 3$

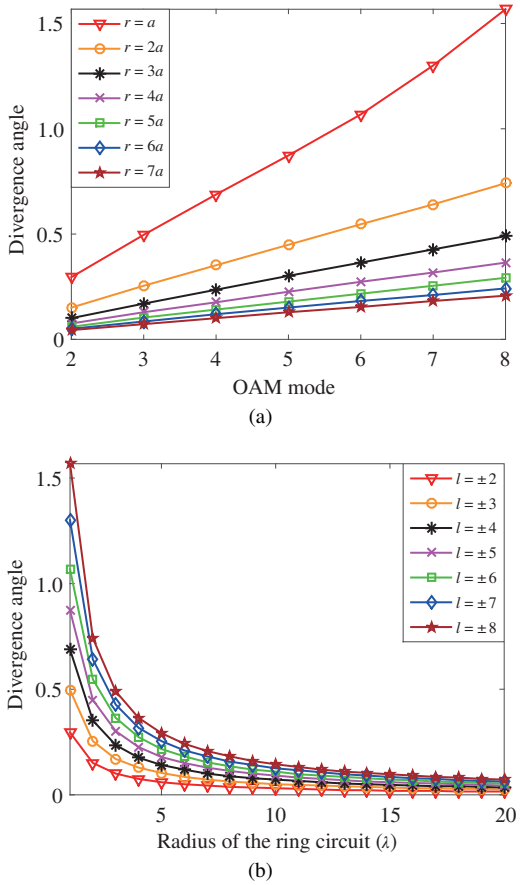

Figure 2 The simulated divergence angles as functions of (a) OAM modes (i.e., $l \in [2,8]$); (b) radii of the ring circuit (i.e., $a = p\lambda$, $p \in [1,20]$)

of the ring circuits are shown in Fig. 2. As shown in Fig. 2(a), the divergence angle is approximately linear with the OAM mode for all cases of radius of the ring circuit. It can be seen from Fig. 2(b) clearly that the divergence angle reduces rapidly as the radius of the ring circuit increases. Moreover, the divergence angles of different OAM modes become comparable to each other as the radius of the ring circuit further increases.

As the radius of the ring circuit increases, the divergence angle of the OAM beam reduces indeed, but in the meantime, more side lobes emerge and the beamwidth of the main lobe decreases. In addition, the significant reduction of the divergence angle becomes impossible as the radius of the ring circuit further increases. Thus all the figures of merits (e.g., the divergence angle, the beamwidth of the main lobe, the power of the side lobe, and the law of diminishing return) should be taken into consideration before determining the radius of the ring circuit.

III. OAM Multiplexing

As demonstrated in sections 1 and 2, the OAM waves possess a null area in the beam center and diverge as the propagation distance increases. Thus it is commonly believed that the OAM multiplexing can only be used in the short-coverage LoS environment. It has been demonstrated that the OAM multiplexing system performs well in the highly reverberant environment if the system is integrated both with spatial equalization and OFDM techniques[21]. However, the highly reverberant environment is quite different from the real multipath environment. For an arbitrary receiving point, the incident waves are distributed over the whole angular range in the highly reverberant environment, while over a certain angular range in the real multipath environment.

In order to have a comprehensive investigation of the angular spread effects on the OAM multiplexing systems, massive OAM multiplexing systems are simulated in the multipath environment with various angular spreads. Specifically, the ring circuit is located in the xOz plane and the OAM beams radiate towards the y-axis. In each system, OAM modes of $\pm l$ (where $l \in [2,7]$) are adopted for multiplexing. The simulated angular spreads (i.e., the angular range of incident waves) range from 0° to 180° with the mean angle along the y-axis. Both the elevation angular spread and the azimuth angular spread are set to the same angular spread.

It is known that the multipath propagation will cause depolarization (e.g., a vertically polarized wave can have horizontal polarized components after scattering) in the real-life environment, thus the simulated incident waves are set randomly polarized and uniformly distributed over a specific angular spread.

In order to evaluate the independent channels of an OAM multiplexing system, we resort the degrees of freedom (DoF)[30,31]. The DoF of a specific multiplexing system can be calculated as

$$\mathrm{DoF} = \frac{\mathrm{tr}(\boldsymbol{R})^2}{\mathrm{tr}(\boldsymbol{R}^2)} = \frac{(\sum_i \lambda_i)^2}{\sum_i \lambda_i^2}, \tag{4}$$

where $\boldsymbol{R} = \boldsymbol{H}^{\mathrm{H}}\boldsymbol{H}$ is the auto correlation matrix of the channel transfer function $\boldsymbol{H}$, the superscript H is the conjugate transpose operator, tr denotes the trace operator, and λ_i represents the ith eigenvalue of $\boldsymbol{R}$. The DoF can represent the correlation of a MIMO antenna (which impacts the diversity order of a MIMO system). Taking an N-port MIMO antenna for instance, the DoF ranges from 1 (totally correlated antennas) to N (totally uncorrelated antennas).

The date transfer rate of a MIMO system depends on the ergodic capacity of an $M_{\mathrm{T}} \times M_{\mathrm{R}}$ channel system (where M_{T} and M_{R} represent the number of antennas at the transmitting and receiving sides, respectively) that can be calculated as[32]

$$C = E\left\{\mathrm{lb}\left[\det\left(\boldsymbol{I} + \frac{\gamma}{M_{\mathrm{T}}}\boldsymbol{H}\boldsymbol{H}^{\mathrm{H}}\right)\right]\right\}, \tag{5}$$

where $\boldsymbol{H}$ represents the channel transfer function of the MIMO system, γ represents the reference signal-to-noise-ratio (SNR), $\boldsymbol{I}$ is the identity matrix, det is the determinant operator, log is the logarithm operator, and E represents the expectation over the random channel $\boldsymbol{H}$.

In order to calculate the DoFs and capacities, ray-tracing simulations[33] are adopted. Specifically, 100 plane waves (that are uniformly distributed over a certain angular spread with the mean angle along the y-axis) carrying narrowband signals are randomly generated and set to impinge on the MIMO antennas. Based on the calculated antenna responses, the corresponding random channel $\boldsymbol{H}$ (i.e., a single realization of $\boldsymbol{H}$) can be obtained. For each angular spread, the capacity of the system is averaged over 10 000 independent channel realizations.

Fig. 3 shows the simulated DoFs and the capacities of the six 2×2 OAM multiplexing systems as functions of angular spread when $a = \lambda$. It can be seen from Fig. 3(a) that the DoFs of all cases are the minimum (i.e., DoF = 1) when the angular spread is 0°. In other words, the two OAM channels of each case are totally correlated. As the angular spread increases, more power is transmitted and received, which results in the increase of DoF. Note that there are two OAM antennas for each case, thus the maximum DoF is 2. Obviously, the two OAM channels are totally independent when the angular spread reaches a certain value. This indicates the crosstalk of the two OAM channels caused by multipath can be completely mitigated by conventional MIMO equalization.

It can be seen from Fig. 3(b) that the capacity starts to increase from 0 when the angular spread reaches a certain value, and the value is larger for the system with higher OAM modes. After a rapid increase of the capacities at small angular spreads, a slow and minor decrease of the capacities can be observed as the angular spread further increases. Finally, the capacities of all cases reach a same value. Since different OAM modes possess different divergence angles, the received power of different OAM modes is different for a specifically small angular spread. As the angular spread increases, the corresponding received power will also increase, which further results in an increasing capacity. The system with higher OAM modes requires a larger angular spread to get rid of 0.

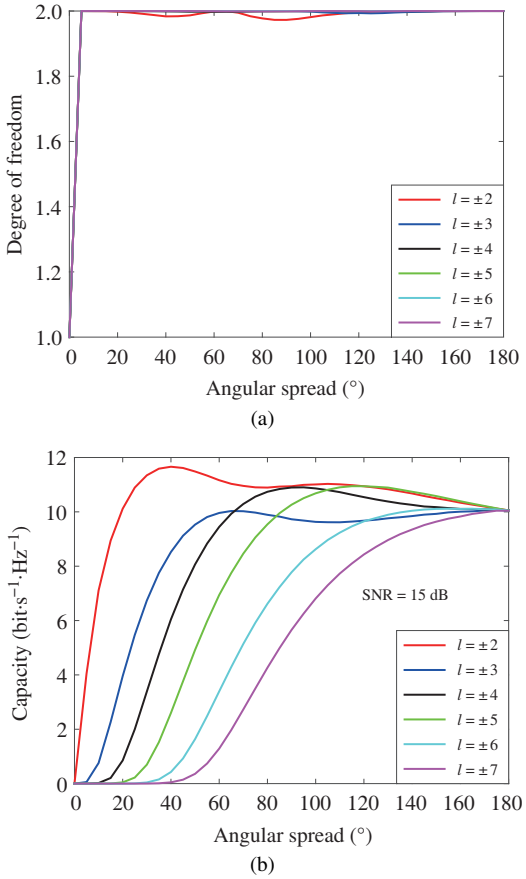

Figure 3 The simulated (a) DoFs; (b) capacities of different OAM multiplexing systems as functions of angular spread when $a = \lambda$

As discussed in section 2 and shown in Fig. 1(a), the gain of the main lobe decreases as the OAM mode increases for a specific radius of the ring circuit. Hence, the maximum achievable capacity is lower for the system with higher OAM modes. When the angular spread goes beyond a certain value, the incident waves cover not only the main lobe but also the side lobes. This explains why the capacities exhibit a slow and minor decrease. It should be noted that the capacity of system with modes $l = \pm 3$ is lower than that of the system with higher OAM modes. This is because the side lobes of modes $l = \pm 3$ possess wider beamwidth and higher side lobe power ratio (as shown in Fig. 1(a)). Interestingly, the capacities of all

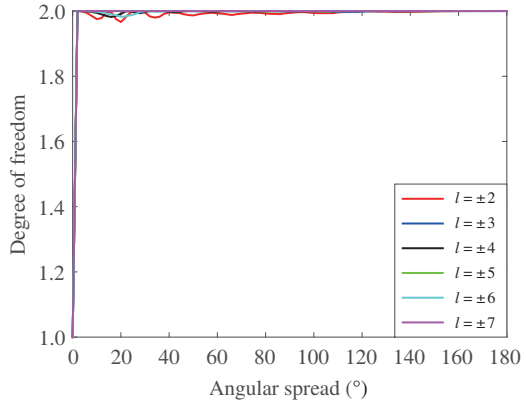

(a)

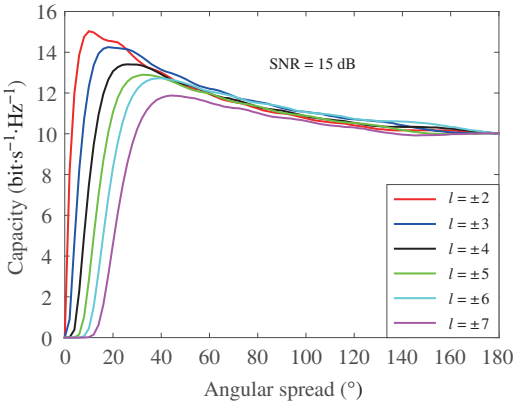

(b)

Figure 4 The simulated (a) DoFs; (b) capacities of different OAM multiplexing systems as functions of angular spread when $a = 4\lambda$

the systems approach to a same value when the angular spread reaches 180°.

In order to show the effect of the radius of the ring circuit on the capacities clearly, OAM multiplexing systems with $a = 4\lambda$ are considered. The corresponding DoFs and capacities are shown in Fig. 4. Same as the previous situation, the DoFs increase to the maximum value (i.e., 2) quickly as the angular spread increases. Compared with the previous situation, the capacities increase much faster and the maximum capacities are larger than that of the case with a small radius. This is because the gain of the main lobe increases and the divergence angle decreases as the radius increases (as shown in Fig. 1(b)). Moreover, since the beamwidth of the main lobe decreases as the radius increases, more obvious and sharper decrease can be observed after the maximum capacities are reached.

For an OAM multiplexing system, the effect of the side lobes should be taken into consideration. Due to the effect of the side lobes, the capacity of the system with $l = \pm 3$ deteriorates seriously when $a = \lambda$. As the radius of the ring circuit increases, the side lobe power ratio decreases obviously (as shown in Fig. 1(b)). Therefore, the deterioration of the capacity of the system with $l = \pm 3$ cannot be observed when $a = 4\lambda$. It can be concluded that the system with OAM modes

Table 1 The elevation angles corresponding to the maximum gain of the main lobes and the maximum capacity (i.e., θ_M and θ_C) for different OAM multiplexing systems when $a = \lambda$, 3λ, and 4λ

l	$a = \lambda$		$a = 3\lambda$		$a = 4\lambda$	
	θ_M	θ_C	θ_M	θ_C	θ_M	θ_C
±2	17°	20°	5.8°	7.5°	4.4°	5°
±3	28.5°	32.5°	9.8°	12.5°	7.4°	10°
±4	39.4°	47.5°	13.6°	17.5°	10.2°	12.5°
±5	50.2°	57.5°	17.2°	22.5°	12.9°	17.5°
±6	61.3°	77.5°	20.9°	25°	15.6°	20°
±7	75°	87.5°	24.5°	30°	18.3°	22.5°

$\pm l$ ($l \in N^+$) suffers less side lobes effect for a larger radius of the ring circuit. It should be noted that the capacities of all the systems also approach the same value as the previous situation. This is because the sidelobe level is roughly the same for all the cases (i.e., all the OAM modes and radii of the ring circuit) when the angular spread is 180°.

To achieve the maximum capacity of a specific OAM multiplexing system in reality, a quantitative and intuitively analysis of the maximum capacities and corresponding angular spread is conducted. The elevation angles corresponding to the maximum gain of the main lobes and the maximum capacity (i.e., θ_M and θ_C) for different OAM multiplexing systems when $a = \lambda$, 3λ, and 4λ are shown in Tab. 1. Obviously, the maximum capacity is achieved when the angular spread (i.e., $2\theta_C$) is slightly larger than $2\theta_M$. Moreover, the difference between θ_C and θ_M is decreasing as the radius of the ring circuit increases. Theoretically, to achieve the maximum capacity, the coming wave should not only cover the maximum gain of the OAM beam, but also avoid to cover the side lobes. This explains why the maximum capacity happens when the angular spread is slightly larger than $2\theta_M$. As the radius of the ring circuit increases, the beamwidth of the main lobe decreases, meanwhile, the decrease of the difference between θ_C and θ_M can be observed.

For an OAM multiplexing system, the inherent maximum capacity can only be achieved when the angular spread is slightly larger than $2\theta_M$. The theoretical maximum capacity can never be achieved if $\theta_M > 90°$. Thus the design and application of the OAM multiplexing system should depend on the real multipath environment (i.e., the angular spread).

IV. Comparison with Conventional Multiplexing System

Two types of 4×4 MIMO systems are considered: the conventional MIMO system and the OAM MIMO system. Specifically, the OAM MIMO system adopts ring circuits with different current phase variations as receiving antennas. The conventional MIMO system adopts the dipole array as receiv-

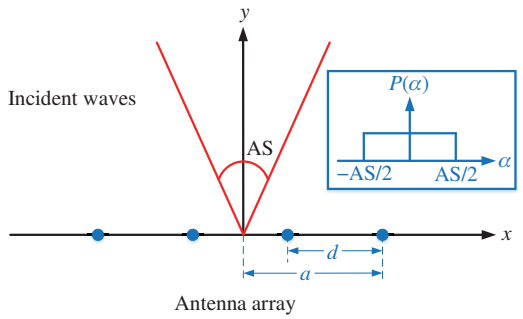

Figure 5 Illustration of the antenna array and incident waves (The distance between two adjacent dipoles is d and the radius of the ring circuit is a. The power spectrum density of the incident wave is uniformly distributed over the angular spreads (AS), while the mean angle is along the y-axis.)

ing antennas, where the array elements (dipoles) are along z-axis and the array axis is x-axis (as shown in Fig. 5). The simulated angular spreads range from 0° to 180° with the mean angle along the y-axis. The incident waves carrying narrowband signals are randomly polarized, and the power spectrum density of the incident wave is uniformly distributed over the whole angular spreads.

Note that the multiplexing system with a larger size (e.g., the radius of the ring circuit and the distance between the array elements) usually has a higher capacity. Therefore, in order to conduct a fair comparison, the diameter of the ring circuit ($2a$) and the size of the dipole array ($3d$) are set to the same value, i.e., $2a = 3d$ (as shown in Fig. 5).

Fig. 6 shows the simulated DoFs and capacities of the conventional multiplexing system and OAM multiplexing systems ($l = \pm 2, \pm 3$, and $l = \pm 3, \pm 4$) when the diameter of the ring circuit and the size of the dipole array are both 2λ. The separation distance between any two adjacent dipoles is $d = 2\lambda/3$. As shown in Fig. 6(a), the DoFs of both OAM multiplexing systems increase rapidly to the maximum value (i.e., 4) once the angular spread is larger than 0, and stay at the maximum value regardless of the increase of angular spread. By comparison, the DoF of the conventional system increases slowly as the angular spread increases, and significant decrease can be observed after it reaches the maximum value. This indicates that the dipoles are not totally independent and the correlation varies with the angular spread, even though the distance between any two adjacent dipoles is larger than the coherence distance. However, the OAM antennas are independent to each other regardless of the angular spreads. Obviously, the OAM multiplexing system outperforms the conventional system in DoF.

As to the capacities, since the dipole antennas do not have null area along y-axis, the capacity is a non-zero value regardless of the angular spread (even when the angular spread is rather small). Even though the capacity of OAM system starts from 0, it increases rapidly as the angular spread increases. When the angular spread increases to a certain value, the capacity of the OAM system with mode $l = \pm 2, \pm 3$ outperforms that of the conventional system. However, the capacity of the OAM system with mode $l = \pm 3, \pm 4$ underperforms that of the conventional system. As the angular spread further increases, a slight decrease can be observed for both conventional and OAM systems. Moreover, the capacities of both systems become comparable and tend to approach a same value.

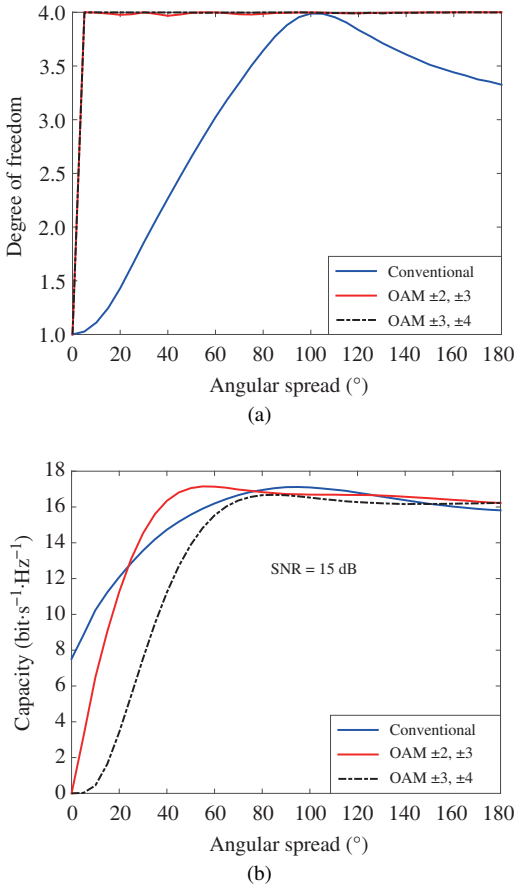

Figure 6 The simulated (a) DoFs; (b) capacities of the conventional multiplexing system (i.e., dipole antennas) and the OAM multiplexing system (i.e., OAM antennas $l = \pm 2, \pm 3$ and $l = \pm 3, \pm 4$) when the diameter of the ring circuit and the size of the dipole array are both 2λ

It has been verified that both capacity and its increment speed of OAM system increase as the radius of the ring circuit increases. Therefore, the OAM and conventional multiplexing systems with a larger size (4λ) are further investigated. Corresponding results are shown in Fig. 7. The DoF of the conventional system increases faster than the former case. Even though there are still slight fluctuations, the significant decrease cannot be observed anymore. However, the DoFs of both OAM multiplexing systems still outperform that of the conventional system regardless of angular spread. As expected and shown in Fig. 7(b), the capacity of the OAM system increases much faster than the small-sized case, and starts to outperform the conventional system at a smaller angular spread. Moreover, the OAM system with $l = \pm 2, \pm 3$ of-

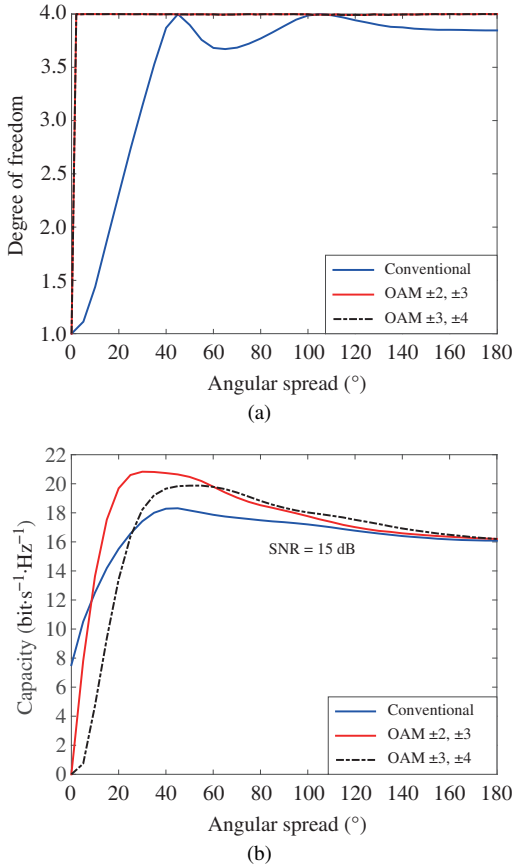

Figure 7 The simulated (a) DoFs; (b) capacities of the conventional multiplexing system (i.e., dipole antennas) and the OAM multiplexing system (i.e., OAM antennas $l = \pm 2, \pm 3$ and $l = \pm 3, \pm 4$) when the diameter of the ring circuit and the size of the dipole array are both 4λ

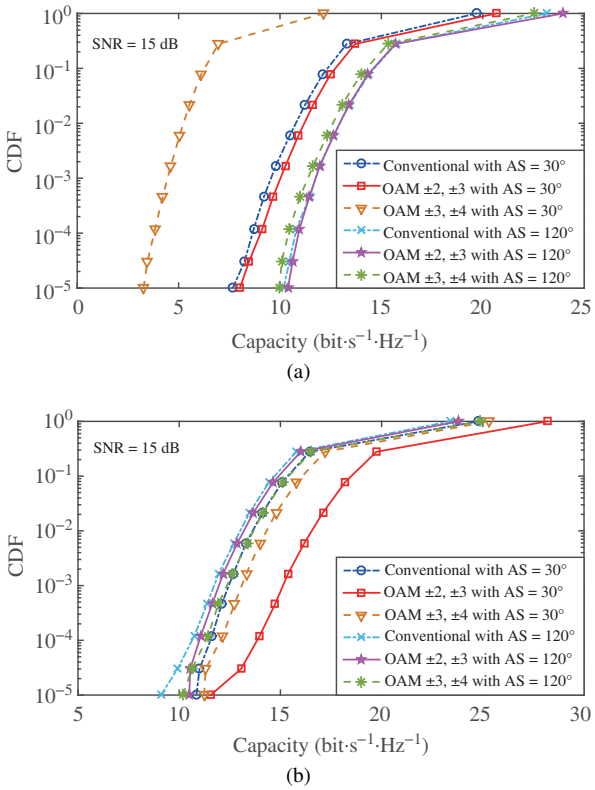

Figure 8 Simulated CDFs of capacities of the conventional and OAM multiplexing systems when the diameter of the ring circuit and the size of the dipole array are (a) 2λ and (b) 4λ in two angular spread cases (i.e., 30° and 120°) when SNR = 15 dB

fers a higher capacity than the conventional system does over a wider range of angular spread, and the OAM system with $l = \pm 3, \pm 4$ even outperforms the conventional system when the angular spread reaches a certain value.

In order to obtain independent channels, the distance between two adjacent antennas should be larger than the coherence distance (i.e., 0.5λ) in conventional multiplexing systems. The capacity will increase as the distance increases. However, when the distance reaches a certain value, it is believed that less gain can be achieved as the distance further increases. Comparing Fig. 6(b) and Fig. 7(b), it can be seen that the capacity gain of the conventional system becomes small as the distance increases from $2\lambda/3$ to $4\lambda/3$. Compared with the conventional system, increasing the radius of the ring circuit can achieve more notable capacity gain.

Note that the capacities of both multiplexing systems are analyzed through the ray-tracing model, which is essentially a statistical method. For a more comprehensive analysis of the capacities, the cumulative distribution function (CDF) of the capacity is further investigated. Fig. 8 shows the CDFs of capacities of the conventional and OAM multiplexing systems in two angular spread cases (i.e., 30° and 120°) when SNR = 15 dB. It can be seen from Fig. 8(a) that the OAM system with mode $l = \pm 2, \pm 3$ outperforms the conventional system in both angular spread cases, while the OAM system with mode $l = \pm 3, \pm 4$ performs worse. Comparing Fig. 8(a) and Fig. 8(b), it can be concluded that capacities of all systems increase as the array size increases. However, the two OAM systems gain more increasement than the conventional system does. As a result, both OAM systems outperform the conventional system in two angular spread cases. The results are in accordance with the findings in Fig. 6 and Fig. 7.

V. Conclusion

In this paper, we investigate the angular spread effect on OAM multiplexing system. It is found that the maximum capacity of OAM multiplexing system can be achieved when the angular spread is slightly larger than the angle corresponding to the maximum gain of the main lobe. Moreover, the maximum achievable capacity increases as the radius of the ring circuit increases and as the OAM order decreases. Extensive simulations are performed to compare the OAM multiplexing system with the conventional system. For the same size of the receiving antennas, both DoF and capacity of OAM system increase faster than that of the conventional system. The ca-

pacity of OAM system outperforms that of the conventional system at small angular spreads. Moreover, compared with the increasing size of the conventional system, the increasing size of the OAM system can achieve more significant capacity gain. Furthermore, we should adopt a specific type of multiplexing system depending on the real multipath environment (i.e., the angular spread). In order to achieve a desirable performance of an OAM system, the order of OAM modes, the radius of the ring circuit, and the real environment should all be taken into consideration. Overall, OAM multiplexing system is a better choice when the angular spread is small (close to the angle corresponding to the maximum gain of the main lobe) or the size of the multiplexing system is relatively large.

REFERENCES

[1] SUN X H, SHAO J F, DAN B, et al. A novel multi-modal OAM vortex electromagnetic wave microstrip array antenna[J]. Journal of Communications and Information Networks, 2019, 4(4): 95-106.

[2] YAN Y, XIE G D, LAVERY M, et al. High-capacity millimetre-wave communications with orbital angular momentum multiplexing[J]. Nature Communications, 2014, 5: 4876.

[3] ZHANG Z F, ZHENG S L, ZHANG W T, et al. Experimental demonstration of the capacity gain of plane spiral OAM-based MIMO system[J]. IEEE Microwave and Wireless Components Letters, 2017, 27(8): 757-759.

[4] ZHANG Z F, ZHENG S L, CHEN Y L, et al. The capacity gain of orbital angular momentum based multiple-input-multiple-output system[J]. Scientific Reports, 2016, 6: 25418.

[5] REN Y X, LI L, XIE G D, et. al. Line-of-sight millimeter-wave communications using orbital angular momentum multiplexing combined with conventional spatial multiplexing[J]. IEEE Transactions on Wireless Communications, 2017, 16(5): 3151-3161.

[6] PARK W, WANG L, BRUNS H, et al. Introducing a mixed-mode matrix for investigation of wireless communication related to orbital angular momentum[J]. IEEE Transactions on Antennas and Propagation, 2019, 67(3): 1719-1728.

[7] CHENG W C, ZHANG W, JING H Y, et al. Orbital angular momentum for wireless communications[J]. IEEE Wireless Communications, 2019, 26(1): 100-107.

[8] LIU K, CHENG Y Q, YANG Z C, et al. Orbital-angular-momentum-based electromagnetic vortex imaging[J]. IEEE Antennas and Wireless Propagation Letters, 2015, 14: 711-714.

[9] CHEN X M, XUE W, SHI H Y, et al. Improving field uniformity using source stirring with orbital angular momentum modes in a reverberation chamber[J]. IEEE Microwave and Wireless Components Letters, 2019, 29(8): 560-562.

[10] EDFORS O, JOHANSSON A J. Is orbital angular momentum (OAM) based radio communication an unexploited area[J]. IEEE Transactions on Antennas and Propagation, 2012, 60(2): 1126-1131.

[11] GUO Z G, YANG G M. Radial uniform circular antenna array for dual-mode OAM communication[J]. IEEE Antennas and Wireless Propagation Letters, 2017, 16: 404-407.

[12] JING H Y, CHENG W C, LI Z, et al. Concentric UCAs based low-order OAM for high capacity in radio vortex wireless communications[J]. Journal of Communications and Information Networks, 2018, 3(4): 85-100.

[13] ZHAO Y F, ZHANG C. Compound angular lens for radio orbital angular momentum coaxial separation and convergence[J]. IEEE Antennas and Wireless Propagation Letters, 2019, 18(10): 2160-2164.

[14] TAMBURINI F, MARI E, THIDE B, et al. Experimental verification of photon angular momentum and vorticity with radio techniques[J]. Applied Physics Letters, 2011, 99: 204102.

[15] WANG H, LI Y F, HAN Y J, et al. Vortex beam generated by circular-polarized metasurface reflector antenna[J]. Journal of Physics D Applied Physics, 2019, 52(25): 255-306.

[16] CHEN M L, JIANG L J, SHA W E I. Ultrathin complementary metasurface for orbital angular momentum generation at microwave frequencies[J]. IEEE Transactions on Antennas and Propagation, 2017, 65(1): 396-400.

[17] YAN Y, LI L, XIE G D, et al. Multipath effects in millimeter-wave wireless communication using orbital angular momentum multiplexing[J]. Scientific Reports, 2016, 6(1): 33482.

[18] JEONG B, KIM H, LEE H. Indoor propagation of electromagnetic waves with orbital angular momentum at 5.8 GHz[J]. International Journal of Antennas and Propagation, 2018, 2018: 1-9.

[19] PAULRAJ A, NABAR R, GORE D. Introduction to space-time wireless communication[M]. Cambridge: Cambridge University Press, 2003.

[20] YANG L, ZHANG W. Hybrid precoding design achieving fully digital performance for millimeter wave communications[J]. Journal of Communications and Information Networks, 2018, 3(4): 74-84.

[21] CHEN X M, XUE W, SHI H Y, et al. Orbital angular momentum multiplexing in highly reverberant environments[J]. IEEE Microwave and Wireless Components Letters, 2020, 30(1): 112-115.

[22] LIANG L P, CHENG W C, ZHANG W, et al. Joint OAM multiplexing and OFDM in sparse multipath environments[J]. IEEE Transactions on Vehicular Technology, 2020, 69(4): 3864-3878.

[23] ZHENG S L, DONG R F, YU X B, et al. Non-line-of-sight channel performance of plane spiral orbital angular momentum MIMO systems[J]. IEEE Access, 2017, 5: 25377-25384.

[24] CHEN X M, ZHANG M, ZHU S T, et al. Empirical study of angular-temporal spectra in a reverberation chamber[J]. IEEE Transactions on Antennas and Propagation, 2018, 66(11): 6452-6456.

[25] WANG L, GE X H, ZI R, et al. Capacity analysis of orbital angular momentum wireless channels[J]. IEEE Access, 2017, 5: 23069-23077.

[26] YAN L, GREGG P, KARIMI E, et al. Q-plate enabled spectrally diverse orbital-angular-momentum conversion for stimulated emission depletion microscopy[J]. Optica, 2015, 2(10): 900.

[27] ZHENG S L, HUI X N, JIN X F, et al. Transmission characteristics of a twisted radio wave based on circular traveling-wave antenna[J]. IEEE Transactions on Antennas and Propagation, 2015, 63(4): 1530-1536.

[28] BALANIS C. Antenna theory: Analysis and designed[M]. 3rd ed. New York: Harper and Row, 2005.

[29] ABRAMOWITZ M, STEGUN I. Handbook of mathematical functions with formulas, graphs and mathematical tables[M]. US GPO (Government Printing Office), 1965.

[30] CHEN X M. Experimental investigation of the number of independent samples and the measurement uncertainty in a reverberation chamber[J]. IEEE Transactions on Antennas and Propagation, 2013, 55(5): 816-824.

[31] PIRKL R J, REMLEY K A, PATANE C S. Reverberation chamber measurement correlation[J]. IEEE Transactions on Electromagnetic Compatibility, 2012, 54(3): 533-545.

[32] FOSCHINI G J. Layered space-time architecture for wireless communication in a fading environment when using multi-element antennas[J]. Bell Labs Technical Journal, 2002, 1(2): 41-59.

[33] GUAN K, LI G K, KÜRNER T, et al. On millimeter wave and THz mobile radio channel for smart rail mobility[J]. IEEE Transactions on Vehicular Technology, 2017, 66(7): 5658-5674.

About the Authors

Wei Xue received his B.S. and M.S. degrees from Xi'an Jiaotong University, Xi'an, China, in 2011 and 2014, respectively. From 2014 to 2018, he was an Avionic Engineer in Aeronautic Computing Technology Institute, Xi'an, China. He is currently pursuing his Ph.D. degree in electronics science and technology, Xi'an Jiaotong University. His current research areas include reverberation chamber, over-the-air (OTA) testing, and statistical electromagnetic.

Xiaoming Chen [corresponding author] received his B.S. degree in electrical engineering from Northwestern Polytechnical University, Xi'an, China, in 2006, and M.S. and Ph.D. degrees in electrical engineering from Chalmers University of Technology, Gothenburg, Sweden, in 2007 and 2012, respectively. From 2013 to 2014, he was a postdoctoral researcher at the same university. From 2014 to 2017, he was with Qamcom Research and Technology AB, Gothenburg, Sweden, where he was involved in the EU H2020 5GPPP mmMAGIC project (on 5G millimeter-wave wireless access techniques). Since 2017, he has been a professor at Xi'an Jiaotong University, Xi'an, China. His research areas include 5G multi-antenna techniques, over-the-air (OTA) testing, and reverberation chambers. He has coauthored 1 book, 2 book chapters, more than 80 journal papers on these topics. Prof. Chen serves as an Associate Editor (AE) of IEEE Antennas and Wireless Propagation Letters (AWPL). He was also a Guest Editor of a Special Cluster on "5G/6G Enabling Antenna Systems and Associated Testing Technologies" in AWPL and a Special Issue on "Metrology for 5G Technologies" in IET Microwaves, Antennas and Propagation. He received the URSI (International Union of Radio Science) Young Scientist Awards in 2017 and 2018, and the IEEE Outstanding AE Awards in 2018, 2019 and 2020.

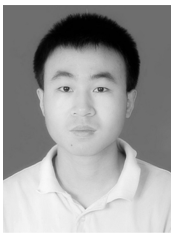

Xiaobo Liu was born in Baoji, China, in 1992. He received his B.Eng. degree in information engineering and his Ph.D. degree in electronic science and technology from Xi'an Jiaotong University, Xi'an, China, in 2014 and 2018, respectively. From 2018 to 2020, he has been a Research Associate with Xi'an Jiaotong University. Since 2020, he has been a Post-Doctoral Fellow in applied mathematics and an Assistant Professor with Xi'an Jiaotong University. He has authored or coauthored more than 20 articles in international and domestic journals and conferences. His research interests include electromagnetic and microwave theory, computational electromagnetics, metasurface, antenna design, and microwave circuit. He serves as a Reviewer for IEEE journals of IEEE Transactions on Microwave Theory and Techniques, IEEE Microwave and Wireless Components Letters, and IEEE Antennas and Wireless Propagation Letters.

Xiangshuai Meng received his B.S. degree in applied physics from Qingdao University of Technology, Qingdao, China, in 2014, and his Ph.D. degree in circuit and system from Xidian University, Xi'an, China, in 2019. He is currently a Postdoctoral Researcher in Xi'an Jiaotong University, Xi'an, China. His research areas include reflectarray, transmitarray, and holographic metasurface.

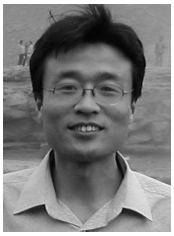

Anxue Zhang received his B.S. degree in electrical and electronics engineering from Henan Normal University in 1996 and M.S. and Ph.D. degrees in electromagnetic and microwave engineering from Xi'an Jiaotong University, Xi'an, China, in 1999 and 2003, respectively. He is currently a professor at Xi'an Jiaotong University. His research interests include antenna and electromagnetic wave propagation, RF and microwave circuit design, and metamaterials, with applications to radar and wireless communications.

Wei E. I. Sha received his B.S. and Ph.D. degrees in electronic engineering from Anhui University, Hefei, China, in 2003 and 2008, respectively. From 2008 to 2017, he was a Postdoctoral Research Fellow and then, a Research Assistant Professor with the Department of Electrical and Electronic Engineering, the University of Hong Kong, Hong Kong, China. In 2017, he joined the College of Information Science and Electronic Engineering, Zhejiang University, Hangzhou, China, where he is currently a tenure-tracked Assistant Professor. From 2018 to 2019, he was a Marie Sklodowska-Curie Individual Fellow with University College London. He has authored or co-authored 102 refereed journal papers, 100 conference publications, 4 book chapters, and 2 books. His Google Scholar citations are 4 030 with an h-index of 27. His current research interests include theoretical and computational research in electromagnetics and optics, focusing on the multiphysics and interdisciplinary research, and fundamental and applied aspects in plasmonics, photovoltaics, metasurfaces, quantum electrodynamics, and computational electromagnetics. He is a Senior Member of IEEE and a Member of OSA. He served as an Editorial Board Member of Progress in Electromagnetics Research and as a Guest Editor for the IEEE Journal on Multiscale and Multiphysics Computational Techniques and Applied Computational Electromagnetics Society Journal. He received the Second Prize of Science and Technology from the Anhui Province Government, China, in 2015, the Thousand Talents Program for Distinguished Young Scholars of China, in 2007, and 4 best student paper prizes and one Young Scientist Award along with his students.